Network Modeling of Flow in a Packed Bed

António A. Martins, Paulo E. Laranjeira, José Carlos B. Lopes, and Madalena M. Dias
Laboratory of Separation and Reaction Engineering, Departamento de Engenharia Química, Faculdade de Engenharia da Universidade do Porto, Rua Dr. Roberto Frias, 4200-465 Porto, Portugal

DOI 10.1002/aic.11047
Published online December 4, 2006 in Wiley InterScience (www.interscience.wiley.com).

The characterization of the flow inside a packed bed requires a full description of the pore geometrical characteristics, and of the flow phenomena at local level. A two-dimensional (2-D) network model for describing the flow phenomena in unconsolidated-packed beds has been developed. The network model consists of two different types of elements: chambers modeled as spheres, and channels modeled as cylinders. The size distributions of the network elements are obtained considering a geometrical model that uses the porosity, and the average-particle diameter as input data. A flow simulator was developed, based on this network model. Results show that since the inertial effects due to connections between channels and chambers are taken into account, this simulator is capable of describing single-phase flow in all the possible flow regimes, from laminar to turbulent. Results also show a good agreement between predicted values of the network model and experimental data available in literature.
 AIChE J, 53: 91–107, 2007
Keywords: porous media, packed beds, network model, nonlinear flow, Ergun equation

Introduction

Transport and flow phenomena in porous media occur in many diverse areas of science and engineering. Many processes in the chemical industry, such as adsorption, ion exchange, chemical and catalytic reactors, are based on or include a packed bed, usually involving the flow of fluids through a porous medium. Better design and operation of these units require a deeper understanding of the mechanisms controlling the transport phenomena inside porous media. Among the different aspects that must be accounted for, the influence of the void space structure is one of the most important.[1,2]

Prediction of process variables, such as the total pressure drop and the total flow rate, are often based on semiempirical correlations with constants that must be fitted to experimental data. In particular, the Ergun equation has become the standard correlation, but other examples include the Kozeny equation, valid for laminar flow, and the Forcheimer equation, valid for nonlinear flow,[3–8] in which the pressure does not vary linearly with the flow rate through the packed bed. Generally, the extension of these correlations to different situations is not possible because they are based on experimental data obtained for a specific system. Also, the study of complex transport phenomena, such as multiphase-flow cannot be done, since no information about the local structure is considered. The inclusion of the local structure increases the adequacy of the model at the cost of greater mathematical complexity.[1,2,9]

Due to the random and very complex structure of many packed beds, a simple approximate model of the pore structure, that preserves the main packing features in a mathematically usable form, must be developed. Different approaches have been proposed to model the structure of the porous space of a packed bed or a porous medium, with different levels of complexity, and using different types of experimental information.[1,2] One type of model describes the flow around the porous-medium particles by defining elementary cells to represent the packed-bed local structure. Initially

Correspondence concerning this article should be addressed to M. M. Dias at dias@fe.up.pt.

these models assumed that each cell is formed by a single particle, where the presence and influence of the nearby particles is accounted for through corrective terms and/or special boundary conditions.[10] Later, the flow was modeled assuming simple structures for the packed bed and its particles. Particularly for regular packings composed of spheres and cylinders, it is possible to obtain analytical expressions describing the flow field inside the packed bed.[11,12] For irregular packed beds and other porous media it is possible to use volume-averaging techniques to describe the flow field.[13] Usually these approaches are applicable with linear flow (characterized by low values of the Reynolds number), high-porosity values, and when a simplified model of the porous medium is considered. Recent evolution in computer power and characterization techniques have allowed the use of the real structure of a porous medium to model-transport phenomena.[14,15]

A different strategy is considered when network models are used. The main objective is to represent the local structure of a porous medium using a set of elements with a geometric shape (such as spheres and cylinders or constricted tubes), simple enough to easily describe their hydrodynamic behavior. The type of elements used may depend on the particle geometry, the porous-medium characteristics, the way the packed bed was constructed, and other relevant theoretical and experimental information. Also relevant to the selection of the elements type are the objectives of the model, and the possibility for solving the model's equations either analytically or resorting to a computer. These models try to balance the trade-offs between an accurate description of the void space inside the porous medium, and the necessary effort to solve the balance equations. Good reviews of network models and their characteristics can be found in the literature.[16,17]

Earlier models assumed that a porous medium could be represented as a tube bundle, with no interconnection between them. The Carman-Kozeny and Ergun equations are based on this model and experimental data of pore-size distributions obtained by porosimetry are usually analyzed with this type of model. Although the relative success of these models to predict the porous medium macroscopic behavior, they are not well suited to describe transport phenomena, where the mixing effects and the local behavior are crucial. Extensions to these models have been proposed in literature.[18–24] Some models assume tubes with constrictions to account for the local variations in the area available to the flow. Others consider that the wall profile varies in a regular way to simplify the resolution of the motion equations. These models are capable of describing the transition between flow regimes, and relate it to the increased effects of expansions and contractions when the fluid velocity rises. However, they do not consider the interconnections between the network elements, which is a severe limitation.

A more realistic description of the local structure involves the definition of a network where the elements are interconnected.[25–29] In 1956 Fatt[30] was the first to introduce network models with interconnected elements to model two-phase flow inside a consolidated porous medium. Initially, and in simpler models, it was assumed that the node volume, corresponding to the interconnections between different network elements, is null. Since in many porous media the nodes correspond to the larger voids, this hypothesis was later relaxed using different approaches. One possibility passes through the definition of two types of elements, for example cylinders and spheres.[25–27] A different approach considers that channels have different zones to represent the expansions and contractions of the real packed bed. Channels may have an assumed shape,[17,31,32] or they can be based on the local geometrical characteristics of the packed bed.[33] A different strategy involves the definition of elements with constrictions. Payatakes et al. [17] introduced the concept of unit cells, based on constricted-tubes. This concept was later used to study single and two-phase flow.[31,32,34,35] In this way the nonlinear effects due to the variation of the flow section can be accounted for, but with an increase on the model complexity. Networks of capillary tubes and of spheres-and-capillaries have been used in simulations of mercury porosimetry,[36–38] and of single and two-phase flow in porous media.[39,40]

Besides the type and geometrical characteristics of the network elements, when a model of this type is used, the knowledge of their size distributions is of fundamental importance. In many studies particular-size distributions are used, mostly without considering the characteristics of the porous medium. In a real packed bed the pore-size distributions depend mainly on the geometrical characteristics of the particles. In the literature one of the preferred ways to determine the local structure of a packed bed involves the creation of the packing by computer simulation. Different hypothesis can be considered during the generation process, in particular, the way the particles are deposited and stability requirements.[25,33,41,42] Detailed knowledge of the packed bed local structure, allows the use of Voronoi Tesselation to determine the equivalent network by assuming a structure for its elements.[43,44] Also, the local structure of the packed bed can be used directly to describe the flow.[14] However, the computational requirements still limit the application of this strategy to packed beds with a small number of particles. Nolan and Kavanagh[45] assumed that the chamber diameters follow to the distribution of spheres that can be fitted inside the network without changing its structure, and that the channels diameters correspond to the distribution of sphere diameters that can percolate through the network. Using these assumptions Nolan and Kavanagh[45] were able to characterize the influence of the particle-size distribution on the pore-size distribution and local structure of the packed bed. Another strategy to determine the pore-size distribution involves porosimetry or image analysis of bidimensional sections after filling the void space with a resin. However, these techniques are not easily applied in packed beds, and in the case of mercury porosimetry the use of high-pressures can destroy the real structure of the original packed bed. Other techniques, such as NMR can be also used,[46–48] however, in many real situations this is not practical due to the high-costs and difficulties involved with the operation of the necessary equipment.

Most of the models referred to earlier are valid or were applied in linear flow. In processes involving packed beds the conditions are such that the flow is often turbulent. A good description of the hydrodynamics in such units is essential for a correct prediction of the pressure drop, and for the design of the auxiliary equipment. This knowledge is also fundamental for the understanding of other phenomena, such as mass trans-

port through a packed bed, mass transfer between phases, and also processes involving chemical reaction.

The main objective of this article is to provide a detailed model of the porous space that, together with a suitable description of the flow, can simulate single-phase in laminar, turbulent and transition regimes and provide a means for evaluating the constants needed in semiempirical correlations. A network model including two different types of elements was selected, since it provides for a simple, but accurate description of the local structure of a packed bed. A geometrical model was developed to determine the characteristic values of the network elements. Although not as rigorous as the Voronoi Tesselation method,[43] the geometrical model developed in this work has some advantages over it, such as the determination of correlation functions only of the porosity of the average size characteristic dimensions of the network elements. In the flow modeling the nonlinear effects are considered explicitly, in order to describe all flow regimes in a packed bed, allowing for the description of the nonlinear regime of the flow in the macroscopic sense. The predictions of the hydrodynamic and geometrical models are compared with correlations and experimental data available data, to assess its validity and determine any parameters that may be necessary to estimate.

Network Model

Although a real porous medium is by definition 3-D, and, consequently, a 3-D network seems to be the natural choice to describe its structure, in this work a 2-D network was used instead. Most correlations available in the literature, supported by experimental data, assume that the flow is essentially 1-D.[2,7] Although, there are some local variations usually associated with the packed bed lateral boundaries, when the ratio between the porous bed and the particle-average characteristic dimensions is large, it can be safely assumed that the velocity profile is essential 1-D.[49–51] This work aims to describe not the local-flow field, but the macroscopic behavior of a packed bed, in particular the total pressure drop as a function of the flow, the main flow regimes, and the transitions between them.

Even considering that the velocity profile is essentially 1-D, in a real packed bed the irregularities of the local structure naturally induce the mixing of the fluid and the existence of a distribution of fluid velocities. A 2-D network is the simplest model that can account for this effects and obtain a meaningful response, yet reducing the computational effort and simulation time. This last effect is of importance when using the model in and industrial context or in optimization studies. Thus, the 2-D network used in this work is the result of a trade-off between the required level of detail, and the effort needed to implement it and solve the resulting system of equations from where the behavior of the packed bed is predicted.

On the other hand, with this network model and for certain geometry characteristics, the flow field in the network can be obtained analytically, and relationships for the main parameters that characterize the macroscopic behavior of the network can be used, avoiding the need to simulate the whole flow field. Under certain conditions, discussed later, this strategy is adequate to describe real systems, even quantitatively.

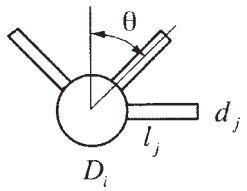

Figure 1. Network unit cell.

Finally, this flow model is the basis for the simulation of other types of transport phenomena inside packed beds, in particular reaction and mass transport. An accurate network model, yet 2-D can keep the computational costs and simulation time at reasonable levels. Even considering the ever reducing computing costs, a simpler model is preferable and easier to modify and to extend for modeling other processes.

The void space inside a packed bed can be described as larger voids interconnected by smaller tube-like voids representing the flow constrictions inside the packed bed.[18,25,33] In this work a 2-D network with two different types of elements is used to explicitly consider these two characteristics. These elements are the chambers, representing the larger voids of the packing, and the channels, representing the smaller voids interconnecting the chambers.

The network is generated by the following set of rules.

1. Each chamber is modeled as a sphere with diameter D_i, and each channel is modeled as a cylinder with diameter d_j, and length l_j.

2. The network is generated from the repetition of a unit cell (see Figure 1) in both x and y coordinates, where x is taken as the main flow direction. The unit cell consists of one chamber, and two or three channels: two oblique channels connecting two contiguous chambers in x and an optional normal channel connecting two contiguous chambers in y. The angle θ between the oblique channels and the x axis is fixed. As a result, the network structure is regular with equal distance between the chamber's centers in each main spatial direction.

3. Additional channels are added to the network flow exit. If the network were generated based only on the repetition of the fundamental cell presented in Figure 1, the chambers at the network exit would have a different coordination number in average from the remaining chambers. The addition of two channels at the network exit ensures that the spatial distribution of the chambers coordination number is not biased.

4. The lateral boundary conditions can be set so that the network simulates either a finite (walled) bed with no lateral channels, or a small part of a larger bed by introducing periodic boundary channels. Figure 2 shows the different types of 4 × 4 (rows × columns) networks that can be generated.

5. The assignment of sizes to each network element is done in a sequential process with:

- To each chamber diameter is assigned a random value following a given size distribution $f_D(D_i)$.
- The channel diameters also follow a given size distribution $f_d(d_j)$, with the restriction that the diameter of any channel must be smaller than the diameters of the two chambers at its extremities. New values of d_j are generated whenever necessary to verify this condition. This implies that the

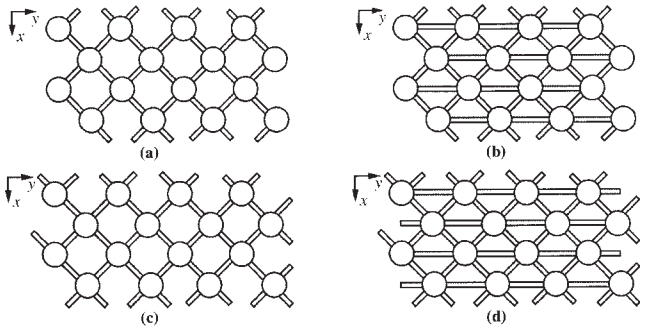

Figure 2. Types of networks that can be generated: (a) no normal and no periodic channels, (b) with normal and no periodic channels, (c) no normal and with periodic channels, and (d) with normal and with periodic channels.

assignment of diameters to each channel is not fully random, and that some correlation between chambers and channels diameters at the local level may occur. When the average values of the distribution functions $f_D(D_i)$ and $f_d(d_j)$ are close, large differences between the initially imposed, and the real channel-diameter distributions could arise due to the application of this restriction.

- The distribution of channel lengths is obtained by fixing l, the average length of an oblique channel, and, therefore, the channel-length distribution depends on the chamber-and channel-size distributions. For the channels located at the entrance and exit of the network, extra chambers are generated at both extremities solely for the purpose of determining the channel length, but these are not considered in the calculation of the void volume of the network or in the flow modeling. For networks with optional normal channels (see Figure 2b and 2d), two different-length distributions, one for the oblique and one for the normal channels, are obtained. Their average values, l and l_n, respectively, are related by $l_n = 2(l + D)\sin\theta - D$.

6. The estimation of some properties, such as the network permeability, requires a value for the thickness of the network δ. Due to the 2-D nature of the network, the value of this parameter depends on the assumptions made. In the proposed model this value is calculated to ensure that the porosity ε, is equal for both packed bed and the network.

7. The connection between a chamber and a channel results in a spherical cap whose volume is common to both elements. When the channels and chambers diameters are similar, this common volume is significant compared with the total void volume of the network, and, thus, in the calculation of the total void space it is only computed once.

Although not required, it is assumed that the functions $f_D(D_i)$ and $f_d(d_j)$ have the same functional form and are nonnegative. The case of monovalued distributions was also considered as a special case for which it is possible to obtain an analytical solution for the flow within the network. The Gaussian distribution is often used as a model to random continuous variables that describe physical phenomena, but it presents the problem of giving a nonzero probability of predicted values of D_i or d_j to be lower than zero, which is physically impossible. Since in many porous media it is observed that the equivalent size distributions are not symmetric, the upper limit log-normal (ULLN) distribution,[37,38] described in the Appendix, was used for both functions.

The networks shown in Figure 2 are regular in the sense that their coordination number C (number of channels associated with a chamber) is almost constant, varying between 4 or 6 for networks with or without normal channels, respectively. To obtain networks with a spatial distribution of the coordination number, chamber and/or channels can be randomly removed, starting from a regular network, until a given average value of C is reached.

In summary, network generation requires the following set of data: number of chambers in the x and y directions; channel and chamber diameters distributions; the channels average length; inclusion or not of normal channels; inclusion or not of periodic boundaries; removal or not of channels or chambers (in which case the average value of C must be given); value of θ; and porosity.

Geometrical Model

The simple geometrical model described here allows a quick and easy estimation of the network elements sizes, from data readily available for packed beds, in particular the porosity and the particle sizes. The main goal of this approach is the determination of correlations for the average characteristic sizes of the network elements. A good estimate for these values ensures that the macroscopic characteristics of the flow field, for example, the total pressure drop, are predicted accurately. The main idea is that from the local structure of regular packings of equal spheres, it is possible to estimate the chambers average diameter, and channels average diameter, and length by defining the equivalent chambers and channels in the regular packings, and ensuring that the porosity between packing and network is maintained. Then, assuming that a real packed bed is an average of the different regular packed beds, correlations can be easily obtained for the average values of the network elements characteristics dimensions.

Using equally sized spheres, six different types of stable regular packings can be constructed,[52] as shown in Figure 3:

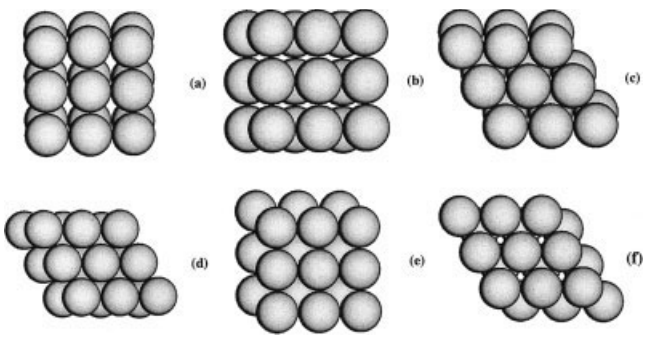

Figure 3. Regular packings of spheres: (a) cubic simple, CUB, (b) orthogonal, ORT, (c) hexagonal, HEX, (d) tetrahedral, TET, (e) rhomboedric body centerd, RBP, (f) rhomboedric hexagonal, RBH.

Table 1. Porosity and Other Network Parameters for Each Regular Packing

Packing	ε	V_{cell}/D_p^3	N_{cham}^{eq}	N_{chan}^{eq}	L_{cell}/D_p
CUB	0.476	1	1	3	1
ORT/HEX	0.395	$\sqrt{3}/4$	1.5	1	$(4+\sqrt{3})/6$
TET	0.302	$\sqrt{3}/4$	1	1.5	$\sqrt{3}/2$
RBP/RBH	0.260	$\sqrt{2}/6$	0.5	2	$(12+6\sqrt{3}+3\sqrt{2}+2\sqrt{6})/36$

Cubic, CUB; Orthogonal, ORT; Hexagonal, HEX; Tetragonal, TET; Rhomboedric Body Centerd, RBP; and Rhomboedric Hexagonal, RBH. The range of porosity values, shown in Table 1, is wide enough to accommodate the porosity values observed in most practical cases. Two pairs of packings, TET/HEX and RBP/RBH, have the same porosity, but apparently, different structures.

For each one of these packings, it is possible to define a fundamental cell that repeats itself in the bed. Packings with the same porosity values can be shown to have the same fundamental cell. From the geometrical analysis of the fundamental cell it is possible, with some simplifying assumptions, to obtain the average values of the chamber diameter, and of the channel length diameter.

The average chamber diameter D, is assumed to be equal to the diameter of the largest sphere that can be fitted inside a cell without changing its shape. With the exception of the CUB packing, this is the diameter of the largest sphere that can pass through a tetragonal face, which is composed with four spheres of equal diameters arranged in such a way that their centers form a square. The opening space between the spheres corresponds to the average chamber diameter, and it can be easily shown that $D = (\sqrt{2}-1)D_p$, where D_p is the diameter of the particles composing the regular packing. For the CUB packing, D is the diameter of the largest sphere that can be fitted inside its fundamental cell, corresponding to a cube with the particles centers placed on its vertices, resulting in $D = (\sqrt{3}-1)D_p$. As a consequence of the previous hypothesis, only two values of D are obtained for the entire range of porosity values, one for $\varepsilon \leq 0.395$ (ORT/HEX, TET and RBP/RBH packings), and another for $\varepsilon = 0.476$ (CUB packing). In order to obtain D for others values of ε, it was assumed that $D(\varepsilon) = \lambda_D(\varepsilon)\ D_p$ where $\lambda_D(\varepsilon)$ has two branches, one for $\varepsilon \leq 0.395$ and the other for $\varepsilon > 0.395$, with a continuous first derivative for $\varepsilon = 0.395$. Considering these restrictions, the following correlation was obtained

$$\lambda_D(\varepsilon) = (\sqrt{2}-1) + 48.44(\varepsilon - 0.395)^2 H(\varepsilon - 0.395) \qquad \varepsilon \leq 0.476 \quad (1)$$

where is the $H(\varepsilon)$ Heaviside-step function.

The average channel diameter d, for each packing, is determined to ensure that the porosity values of the fundamental cell and the packing are equal. The number of equivalent channels is equal to the number of tetragonal faces for the CUB packing or to the number of triangular faces for the remaining regular packings. A triangular face is formed with three spheres of equal diameter arranged in such a way that their centers are the vertices of an equilateral triangle. These two conditions require the definition of the equivalent number of chambers N_{cham}^{eq}, and channels N_{chan}^{eq}, associated with the fundamental cell for each packing. These values, as well as the dimensionless cell volume V_{cell}/D_p^3, are shown in Table 1.

The average channel length l, is obtained by fixing the same pressure gradient in both the network and the geometrical model, that is, assuming an equal distance between the centers of two chambers located in adjacent rows L, and the centers of two spheres in adjacent layers L_{cell}. The dimensionless distance between the centers of spheres L_{cell}/D_p, is also shown in Table 1.

To close the calculation of d, an estimation of θ is also necessary. Defining the tortuosity T, as the ratio between the porous bed length and the actual passage length, and considering the regular structure of the network, it can be shown that the following relation between θ and T holds

$$\theta = \arccos T \quad (2)$$

T is usually considered as a macroscopic parameter, and for actual packed beds, local variations in the value of θ are expected, but, in this article, an average value is assumed. The parameter T is a function of the porous medium characteristics, and for packed beds it is usually correlated as a function of porosity.[53,54] A correlation based on experimental data obtained for packed beds formed by spheres with a narrow-size distribution[53] was considered in this work, in the form

$$1/T = 1 - 0.49 \ln \varepsilon \quad (3)$$

For each packing, the values of d and l can be determined by solving a nonlinear system of two equations. Correlation functions of the type $d(\varepsilon) = \lambda_d(\varepsilon)D_p$ and $l(\varepsilon) = \lambda_l(\varepsilon)D_p$, valid for the whole range of porosity values were obtained

$$\lambda_d(\varepsilon) = 0.4142 - 0.2522 \exp\left[-\frac{(\varepsilon - 0.260)}{0.0703}\right] \quad (4)$$

$$\lambda_l(\varepsilon) = 1.072 - 1.892(\varepsilon - 0.26) + 53.18(\varepsilon - 0.26)^2 - 237.1(\varepsilon - 0.26)^3 \quad (5)$$

All three correlation functions are shown in Figure 4. Comparing the curves for $\lambda_D(\varepsilon)$ and $\lambda_d(\varepsilon)$, it is observed that, for porosities around 0.4, the geometrical model predicts a nearly equal value for the average chamber and channel diameters. In these conditions the application of the restriction between the chambers and channels diameters at the local level can lead to some segregation between both distributions.

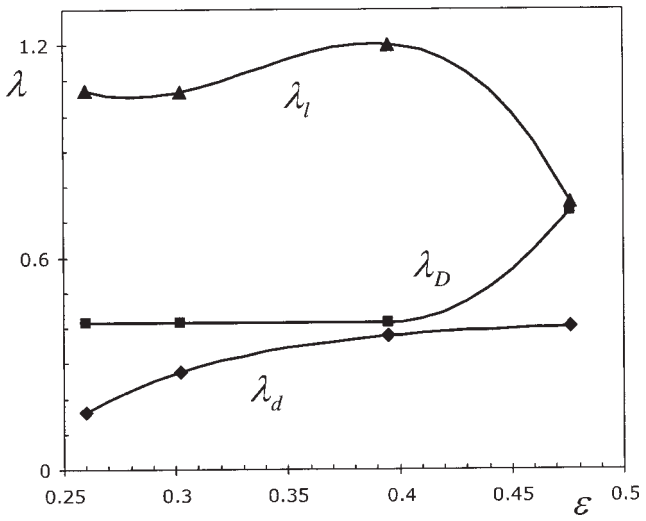

Figure 4. Values of $\lambda_D(\varepsilon)$, $\lambda_d(\varepsilon)$ and $\lambda_l(\varepsilon)$ predicted by the geometrical model and respective correlation curves.

This model can be extended to packings with narrow* particle-size distributions $f_{D_p}(D_{p,i})$, in which case the elements-size distributions can be obtained using the following expressions

$$f_D(D_i) = \lambda_D(\varepsilon) f_{D_p}(D_{p,i}) \tag{6}$$

$$f_d(d_j) = \lambda_d(\varepsilon) f_{D_p}(D_{p,i}) \tag{7}$$

Results obtained on simulated random-packed beds made from spheres with a given size distribution show that only when the size distribution of the particles size is narrow, it is valid to define an average value for the channels and chamber diameters. Using a narrow particle-size distribution, Chan and Ng[41,55] obtained $\lambda_d = 0.38$ and $\lambda_D = 0.45$. For simulated-packed beds with $\varepsilon \approx 0.40$, these values show a good agreement with the ones predicted by the geometrical model. The channel-length distribution was determined by Chu and Ng[33] for simulated-packed beds, taking into consideration the influence of a limiting wall. Results show that for $\varepsilon \approx 0.40$, $\lambda_l \approx 1.25$, which is also in good agreement with the predictions of the geometrical model.

Other studies,[56,57] in which mercury penetration in packed beds formed by spheres with a narrow-size distribution and a regular structure was studied, showed that the size distribution of the constrictions between the sphere equivalent to the channels is very narrow. Therefore, for a packed bed with a random structure, but formed by particles with a monosized distribution, the pore-size distributions can be considered monovalued within a small error. For the range of porosity values considered in this work, values of λ_d ranging from 0.27 and 0.37 were obtained.

Two datasets for packed beds from Payatakes, Tien and Turien,[18] referred as PTT1 and PTT2, were used to obtain values of the average chamber and channel diameters and the channel length as shown in Table 2. The first dataset consisted of nearly spherical glass beads with uniform size; the second is composed of sand grains with a narrow distribution of sizes. Since the particle-diameter distribution is not available, only the reported average-particle size and bed porosity were considered in the calculations. Based on a model of constricted capillaries, these authors calculated the diameters of constrictions (channels) and expansions (chambers) using data for the penetration of water in packed beds. A good agreement is observed for the calculated value of in the datasets PTT1 and PTT2, with an error of about 7% between the two values. The values of D and l show larger deviations that can be attributed to the different structures assumed to the packed beds in both models. The geometrical model was also used for six other sets of data from Kim[58] that were used to compare experimental data with results predicted by the network model later in this article.

Although the comparison between predicted and experimental values is quite good for packed beds made from spherical particles with a narrow particle-size distribution, a drawback of this model concerns the determination of the average value for the coordination-number distribution C. The geometrical model assumes that the calculated values are independent of C, and although it is possible to define C for each fundamental cell, the difference of structure between the equivalent network and the regular packings, and the one considered in this work precludes the use of this approach.

Flow Simulation

The flow through the network is modeled using the analogy with an equivalent electric circuit.[31,32] It is assumed that: the flow is isothermal, incompressible and steady-state; the chambers behave as perfect mixers; and the gravitational effects are negligible. Figure 5a shows a representation of the electric analogue for the network represented in Figure 2d. The flow analogy in each channel, represented in Figure 5b, is given by

$$p_i - p_{i-1} = \Delta p_j = R_j q_j \tag{8}$$

where p_i is the pressure at node given by the center of chamber i, Δp_j is the pressure drop across the branch associated with the channel j, q_j is the flow rate through channel j, and R_j is the hydraulic resistance associated to channel j.

Using Kirchoff's laws and standard resistive network analysis[31,59] a system of algebraic equations is obtained, which can be solved to obtain the pressure at each node, by imposing either the total pressure drop Δp_T, or the flow rate q_T, across the network. The nature of this system depends on the flow characteristics, and terms considered in the description of the flow inside each network element. In the more general case, R_j depends on the channel flow rate, and the resulting system of equations is nonlinear, and it is solved using a fixed-point iteration method.[60] The initial estimate is obtained considering that the flow is laminar in all channels, and that R_j is independent of q_i. Under these conditions the system of equations is linear and can be easily solved.

*For wide distributions, the smaller particles can settle in the voids by the larger particles, drastically reducing the total porosity of the packing, and the structure of the void space. Under these conditions, this model is not expected to give reliable results.

Table 2. Experimental Data and Calculated Values for the Network Elements Average Sizes

	Experimental Data					Geometrical Model			
Set	ε	D_p (mm)	d (mm)	D (mm)	l (mm)	d (mm)	D (mm)	l (mm)	θ (rad)
PPT1	0.40	0.470	0.177	0.379	0.469	0.179	0.196	0.563	0.808
PPT2	0.47	0.714	0.260	0.614	0.715	0.287	0.490	0.588	0.753
KIM1	0.357	2.10	–	–	–	0.737	0.870	2.46	0.844
KIM2	0.360	3.07	–	–	–	1.08	1.27	3.61	0.841
KIM3	0.359	4.10	–	–	–	1.45	1.70	4.82	0.842
KIM4	0.348	3.69	–	–	–	1.26	1.53	4.26	0.851
KIM5	0.344	3.28	–	–	–	1.11	1.36	3.76	0.854
KIM6	0.342	2.76	–	–	–	0.926	1.14	3.16	0.856

In the case of a network with monosized elements, a uniform network, with periodic boundary conditions, the pressure drop in each branch Δp_j is constant, and an analytical relationship between the Δp_T and q_T can be obtained

$$\Delta p_T = \sum_{j=1}^{N_x+1} \Delta p_j = (N_x + 1)\Delta p_j = \frac{N_x + 1}{2N_y} R_j q_T \tag{9}$$

In the description of the flow inside the network the existence of two types of elements must be considered explicitly. Chambers and channels have different geometrical characteristics, resulting in different hydrodynamic behavior. In both cases, a network element is equivalent to a resistance to the flow, which depends on its characteristic dimensions. According to the hypothesis considered on the definition of the network elements, based on the correspondence between them and on the local structure of a packed bed, different mechanisms and resistance terms are assigned to the two types of network elements.

Modeling the channels behavior

The channels represent the constrictions between the packing particles and when the flow is slow, they represent the main term of resistance to the flow, which is due to the friction of the fluid on the packed bed particles, corresponding to the channel walls on the network model. This friction resistance R_j^F, can be expressed in the following general form[61]

$$R_j^F = \frac{8\rho f_j q_j l_j}{\pi^2 d_j^5} \tag{10}$$

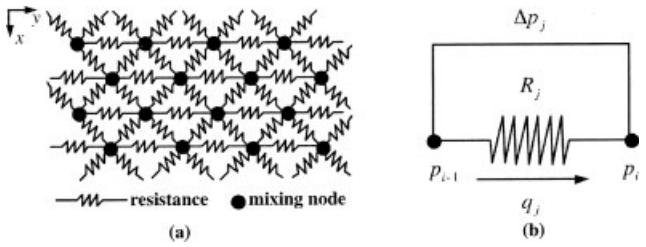

Figure 5. Electric analogue used in single-phase flow simulation: (a) electric circuit equivalent to the network in Figure 1d, and (b) analogy for flow in a branch of the network.

Where q_j is the flow rate through channel j, f_j is the friction factor, that depends on the channel-Reynolds number

$$\mathrm{Re}_j = \frac{4\rho q_j}{\pi \mu d_j} \tag{11}$$

and ρ and μ are the fluid density and viscosity, respectively.

For laminar flow $\mathrm{Re}_j < \mathrm{RE}_j^{Min}$, Poiseuille's relationship $f_j = 64/\mathrm{Re}_j$, can be replaced in Eq. 10 to obtain

$$R_j^F = \frac{128\mu l_j}{\pi d_j^4} \tag{12}$$

For turbulent flow $\mathrm{Re}_j > \mathrm{Re}_j^{Max}$, Blasius equation $f_j = 0.3164\ \mathrm{Re}_j^{-0.25}$, is used.

In the transition zone $\mathrm{Re}_j^{Min} \le \mathrm{Re}_j \le \mathrm{Re}_j^{Max}$, there are no analytical expressions for f_j as a function of Re_j. Experimental data available in literature[62] show that this zone ranges from 1,500 to 7,000 in terms of values, with some scattering on the values of f_j. However, to determine the flow and pressure field inside the network it is convenient to have an analytical expression that provides f_j (Re_j) for the transition zone, and this will be obtained by interpolation between the laminar and turbulent regimes as shown in Figure 6. A linear interpolation scheme assuming that $\mathrm{Re}_j^{Min} = 2300$ and $\mathrm{Re}_j^{Max} = 5000$, values typically considered as the limits of the transition zone, results in $f_i = 0.0195 + 3.63 \times 10^{-6}\ \mathrm{Re}_j$, and is used in the case of uniform networks where the flow can be determined analytically. However, the previous expression is not always adequate because it introduces discontinuities in the first derivative of f_j (Re_j). For nonlinear flow conditions, the problem solution involves a nonlinear system of equations, and if most of the channels are in the transition regime, it may be difficult to obtain convergence.

Therefore, an interpolation scheme based on Tchebyshev polynomials is also implemented, ensuring continuity between the laminar/transition and transition/turbulent flow regions for both functions, and the first and second derivative values. Tchebyshev polynomials were chosen so that the interpolated values were similar to those obtained by linear interpolation, and, thus, it was imposed that for $\mathrm{Re}_j = 3{,}650$ both interpolation functions give the same value. Values of $\mathrm{Re}_j^{Max} = 6175$ and $\mathrm{Re}_j^{Min} = 1586$ were obtained from the interpolation polynomials, close to the transition zone limiting values of the obtained from experimental data available in the literature, and in agreement with the values of 5,000 and 2,300 considered before for the linear interpolation scheme, and normally considered in the literature as the limiting values for the transition zone.[62]

Modeling the chambers behavior

The connections between chambers and channels represent the contractions and expansions experienced by the fluid when passing from one type of network element to the other. The resistance to the flow results from the change in fluid velocity.

In a real porous medium the changes in the flow area may be smooth or sudden. In the network model, as a first approximation and to simplify the chambers hydrodynamics, it is assumed that the variations of the flow area are sudden. With this condition it is possible to solve the mass and momentum conservation inside a chamber and associated channels, and to determine the resistance to the flow due to the expansions and contractions, and their dependence on the geometrical and flow characteristics at the element level. In this work, a different and simpler approach is considered.

The resistance term associated with the expansions and contractions R_j^E, is considered to be the sum of two terms. The term for laminar flow R_j^{EL}, is independent of the flow rate, and was derived by Koplik[28]

$$R_j^{EL} = \frac{512\mu}{\pi^2 {d_j}^3} \tag{13}$$

The earlier expression is in fact twice the one derived by Koplik,[28] since in this case each channel is connected with two chambers. A similar expression has been used for linear flow in a network model, where both channels and chambers are assumed to be prisms of rectangular cross-section.[29] The second term R_j^{ET}, represents the nonlinear flow contribution, and is approximated by

$$R_j^{ET} = \frac{8\rho q_j}{\pi^2 d_j^4}(K_j^{in} + K_j^{out}) \tag{14}$$

where K_j^{in} and K_j^{out} are analogous to the coefficients for sudden expansions and contractions, respectively, generally used in the calculation of pressure losses in pipe systems.[62] Correlations for these coefficients are available in the literature for the case of one channel with a single entrance or exit of fluid from the chamber. In this work, the values of K_j^{in} and K_j^{out} are replaced by their sum, represented by K_j. In a real packed bed, K_j may depend on the geometrical and flow-field characteristics of the elements at local level, and it could be determined through direct modeling of the flow in a chamber with inflow and outflow channels, using for example CFD modeling. However, for sake of simplicity, in this work it is assumed that $K_j = K$ is independent of the local geometrical and flow-field characteristics, thus, constant throughout the network. Assuming that the chambers diameters are much larger than the channels diameters, and that mixing of streams inside the chambers is not significant, then $K \approx 1.5$.[62] In a real packed bed, a higher value of K is expected to account for the mixing of the fluid in the chambers, the existence of more than one entrance and exit in most chambers of the network, and the different ratios between the diameters between the channels and chambers associated with each other. The value of this parameter can be estimated from experimental data for nonlinear flow, as it will be shown later.

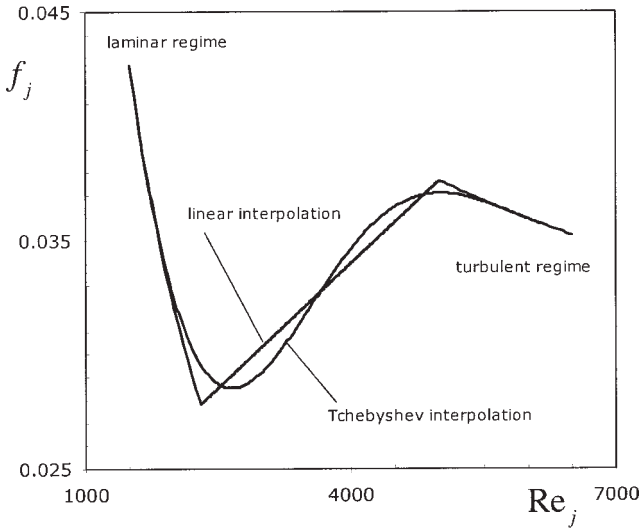

Figure 6. Plot of friction factor f_j, as a function of the Reynolds number Re_j, comparing the linear and Tchebyshev interpolation functions for the transition zone.

A similar approach was also considered in the works Blick,[19] Thauvin and coworkers[26,27] and Niven[63] to describe flow in porous media for linear and nonlinear flow. These studies show that the transition between the two flow regimes can be attributed to an increase on the importance of the expansions and contractions in the flow through a porous medium. However, with the exception of the work of Blick,[19] no attempt was made in these studies to correlate the parameters related with the expansions and the contractions with the macroscopic characteristics of the porous medium, for example, porosity and particle-size distribution, as performed in this work.

Analysis of the proposed model

To model the flow inside the network, the network is assumed as being composed of branches, each of them formed by a channel and two half chambers at its extremities, and mixing nodes, with no volume and negligible resistance to the flow. The overall resistance to the flow for the branch associated with channel j is given by

$$R_j = R_j^F + R_j^{EL} + R_j^{ET} \tag{15}$$

that is, the flow resistance of the mixing nodes is negligible, and the resistance due to the connections between chambers and channels is associated with the network branches.

Which resistance term is dominant depends on the flow conditions inside the network elements. In linear-flow regime, the flow rate is very small, and it is possible to assume that $R_j \approx R_j^F + R_j^{EL}$, and, thus, independent of the flow rate (Eqs. 12 and 13). Under these conditions the pressure drop is proportional to the flow rate, and the value of permeability can be easily obtained. In fully developed nonlinear flow, the term R_j^{ET} is dominant, and the pressure drop is proportional to, leading to a macroscopic nonlinear-flow regime for the

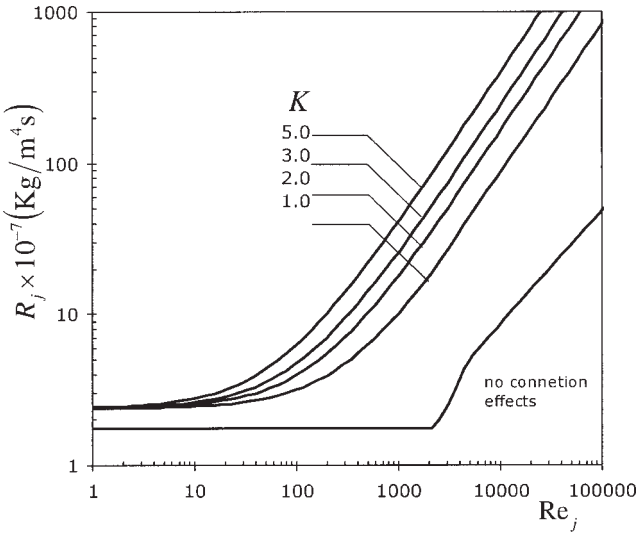

Figure 7. Plot of overall channel resistance R_j, as a function of the Reynolds number Re_j, for different values of K, including the situation without connection effects between channels and chambers.

flow through the network and, consequently, in the equivalent packed bed.

Figure 7 shows as a function of Re_j, for different values of K, where the case without considering the connections effects ($R_j^{ET} = R_j^{EL} = 0$) is also shown in order to compare and determine under which conditions friction is dominant. For $\mathrm{Re}_j \leq 1$, both curves have similar behavior with the difference in values resulting from the inclusion of the term R_j^{EL} when the effects of the connections are considered in linear flow. Increasing the value of Re_j, the two curves start to behave differently, due to the increase in importance of the term R_j^{ET}. For values of $\mathrm{Re}_j > 1{,}000$, this term is dominant, and the transition between the two zones is smooth. When only the friction effects are considered, the transition is abrupt, a consequence of how f_j varies with Re_j, and the value of resistance is much lower. From a qualitative standpoint, the behavior predicted by the full model[64,65] seems to be more adequate, but only with the actual simulation of the flow field inside a network, it is possible to draw conclusions, as it will be shown later in this article.

An analysis of the expressions obtained shows that the channel diameter is the controlling parameter of the resistance value, and that the dependence on the value of d_j is similar for all terms, although smaller for R_j^{EL}. Also, the terms R_j^F and R_j^{EL} can be considered as friction terms, as they depend on the viscosity of the fluid, and R_j^{ET} can be seen as an inertial term, as it depends on the fluid density. Assuming that the transition between linear and nonlinear flow in the channels (not the network branches) occurs for a value of $\mathrm{Re}_j \approx 2300$,[62] the results presented in Figure 7 show that the term R_j^{ET} is dominant even when the flow in the network channels is laminar. Therefore, it is possible to have conditions of nonlinear flow inside the network before the transition to turbulent flow, in agreement with the conclusions of previous authors.[1]

Results of the Hydrodynamic Model

Simulations were carried out using the network model described earlier in order to study the effect of various model parameters on the network hydrodynamic behavior. First, the impact of the network dimensions is discussed. Then, the influence of the connections between chambers and channels are analyzed, as well as the influence of the geometrical characteristics of network and its elements. Finally, the geometrical model is used to estimate the network elements size distributions, allowing the comparison between predicted values with experimental data available in the literature.

The raw results of a network and flow simulation provide information on the pressure and flow field in the network, but for the sensibility analysis and the comparison of experimental data and simulated values, three parameters are used. The first parameter is the network permeability, obtained in laminar regime as

$$k = \mu \frac{L_x}{L_y \delta} \frac{q_T}{\Delta P_T} \tag{16}$$

where L_x and L_y are the length of the network in the main and the normal directions to the flow, respectively.

The other two parameters are the constants A and B obtained by writing the Ergun equation[3] as $F^* = A/\mathrm{Re}^* + B$ where F^* and Re^* are the modified-friction factor, and the modified-Reynolds number, respectively, and can be determined from

$$F^* = \frac{L_y^2 \delta^2}{L_x} \frac{\Delta P_T}{\rho {q_T}^2} \frac{D_p \varepsilon^3}{(1-\varepsilon)} \tag{17}$$

$$\mathrm{Re}^* = \frac{\rho}{\mu} \frac{q_T}{L_y \delta} \frac{D_p}{(1-\varepsilon)} \tag{18}$$

The values of these two constants can be predicted from the results of the network model and compared with values obtained from the literature; for example Ergun[3] obtained $A = 150$, and $B = 1.5$, and later, Macdonald and coworkers[4] with a larger experimental database suggested $A = 180$, and $B = 1.75$.

Influence of the network size

The network elements-size distributions are based on probability-density functions, and, therefore, it is necessary to determine the network size that ensures that the sample, and the results are statistically significant. Figure 8 shows the network permeability k, as a function of N_y, for three values of N, using networks with normal channels and periodic boundaries, with $d = 0.002$ m, $D = 0.004$ m, $l = 0.007$ m and $\theta = \pi/4$. For each pair of N_x and N_y values, 12 simulations were performed, varying the numerical value of the seed of the random number generator. The values of are determined imposing a low value for ΔP_T, and $K_j = 0$, so that the flow is laminar without nonlinear effects in all network branches. Two-size distributions with different standard deviations σ_D and σ_d, were considered, and results show that, in both cases, if $N_x \geq 100$ and $N_y \geq 100$, the permeability values tend to a limit value and can be considered to be statistical significant, that is, the spread in the permeability val-

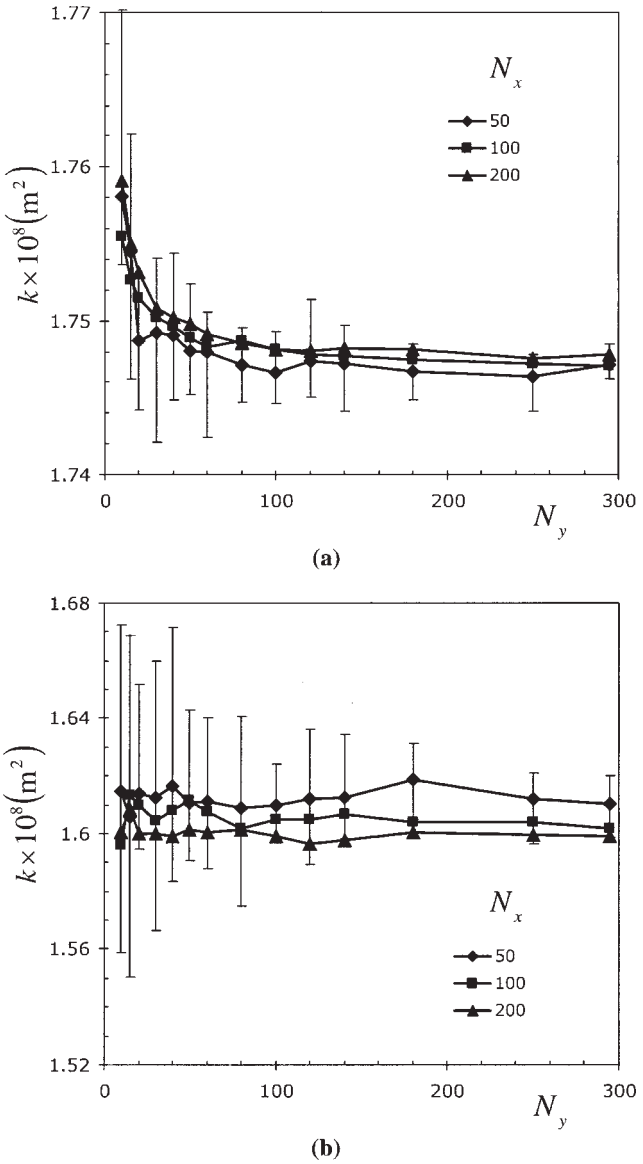

Figure 8. Network permeability *k*, as a function of *Ny*, for three values of N_x, for networks with normal channels and periodic boundaries, for two distributions: (a) $\sigma_D = \sigma_d = 0.05$, and (b) $\sigma_D = \sigma_d = 0.40$.

ues is less than 1% from its mean value. A larger spread is obtained for higher-values of the standard deviation, resulting from a wider distribution of the network element sizes that influences the flow and pressure fields in the network.

The same behavior is observed, independently of the value of C, the inclusion or not of normal channels, type of boundary and flow regime, and for other values of the network parameters. Therefore, based on the previous results, most of the simulations shown in this article were obtained for $N_x \times N_y = 100 \times 100$ networks with periodic boundary conditions and channels normal to the flow. For the network elements it was generally used $d = 0.002$ m, $D = 0.004$ m, $l = 0.007$ m, $\theta = \pi/4$, $\sigma_D = \sigma_d = 0.40$ and $\varepsilon = 0.4$. When using the full model to calculate resistance to the flow of the network elements the value was assumed. When different values were used, they are explicitly stated in the text.

Influence of chamber/channel connections effects

The inclusion of the connection effects between chambers and channels, in addition to the usual terms corresponding to friction of the fluid on the channels walls, is one of the main features of the network model proposed in this work. To assess the significance of these effects on the behavior predicted by the network model, Figure 9 plots F^* vs. Re_j for three situations: connections effects for both linear and nonlinear regimes; connections effects for linear regime only, that is, $R_j^{ET} = 0$ and $K = 0$; and no connection effects, that is, $R_j^{ET} = R_j^{EL} = 0$.

For low-values of Re*, corresponding to linear flow, similar behavior is predicted in all three cases, with a small difference occurring due to the inclusion or not of R_j^{EL}, the resistance term associated with the connections in laminar regime.

When R_j^{ET} is included, major differences are observed in the three plots, namely for values of Re* corresponding to the transition and turbulent regimes, showing that for fully developed nonlinear flow R_j^{ET} becomes the dominant term, and F^* tends to a constant value. Figure 9 also shows Ergun equation with the set of constants proposed by Macdonald and coworkers,[4] and it is clear that only when the effects of the connections between chambers and channels are considered, the predicted behavior is in agreement with Ergun equation.

Influence of network geometry parameters

Three characteristics can be changed in the geometry of the proposed network model: the nature of the network boundaries; the angle θ; and the distribution of chamber coordination numbers.

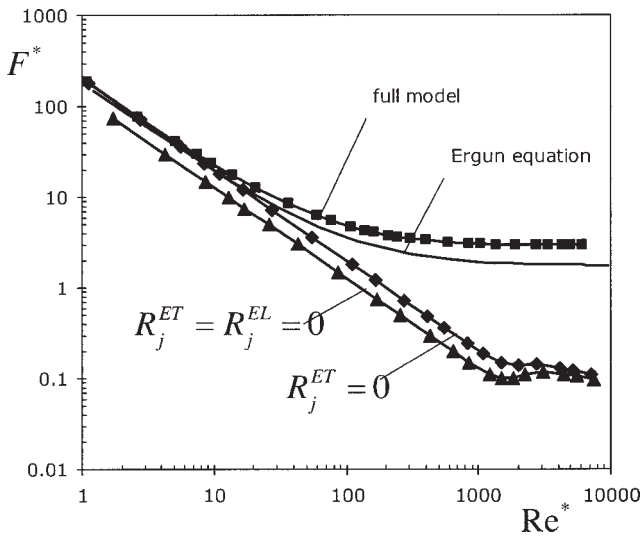

Figure 9. Plot of modified friction factor *F vs. the modified Reynolds number Re*, with and without the effect of the connections between chambers and channels.**

For networks with dimensions considered to be statistically significant, the difference in the total number of elements between a network with or without periodic boundaries is very small. Thus, the effect of the network boundaries may be significant only when the total number of elements is small.

Neither of the resistance terms R_j^F, R_j^{EL} or R_j^{ET} is a function of θ and, therefore, this parameter has no influence on the modeling of the flow. On the other hand, parameters that depend on the geometrical characteristics of the network, such as the permeability, may show a dependence on θ. Nonetheless, increasing θ keeping l fixed will increase the length of the network in the x-axis direction, and decrease the length of the network in the y-axis direction. The two effects compensate each other, resulting in values of δ that have a small dependence on θ, leading to a negligible influence on the value of the permeability, and other parameters that are functions of δ.

The distribution of chamber-coordination numbers C_i, can be modified in two ways: the inclusion or not of normal channels, leading to average-coordination numbers of $C = 4$ or $C = 6$, respectively; and the removal of chambers and/or channels. The influence of the spatial distribution of values of C_i is observable on two scales. At the network element level, changes in the number of channels associated with a given chamber influence the local flow field. This is particularly important when the channel removal process includes the oblique channels, since they are the network branches representing the main resistance to the flow in the network. At the macroscopic level, the total void volume of the network depends on the total number of elements, which leads to changes in δ, affecting the values of macroscopic parameters, such as the permeability and the constants A and B.

Figure 10 shows the distribution of fluid velocities in each type of channel v_j, for networks with or without normal channels, expressed in the form of a histogram with 30 classes, where N_v is the number of channels with a velocity value within a certain range. Results were obtained without removal of channels and/or chambers and under linear flow conditions. The values of v_j for the normal channels are

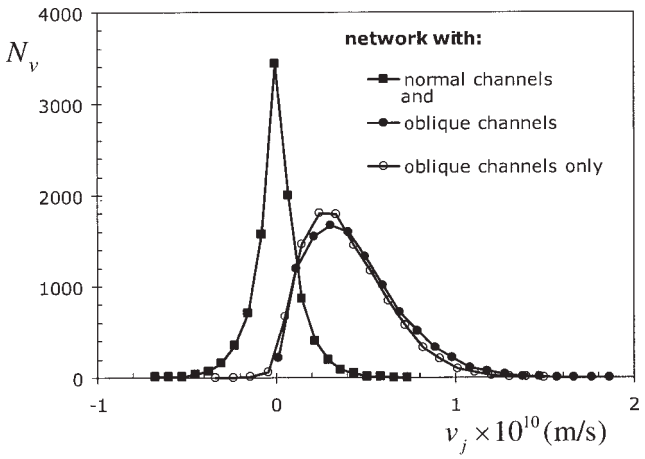

Figure 10. Distributions of the channel fluid velocity v_j, for networks with and without normal channels under linear-flow conditions.

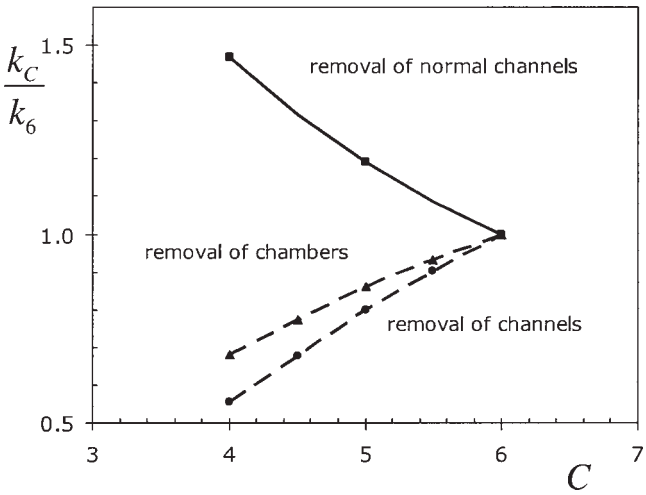

Figure 11. Ratio between k_6, the network permeability at $C = 6$ and k_c, the network permeability at C, as a function of the mean-coordination number C.

smaller and show a Gaussian-like behavior centerd at zero-velocity. The velocity distributions for the oblique channels are identical, regardless of the existence or not of normal channels, showing that the network branches with oblique channels control the network hydrodynamic behavior.

The influence of the coordination number on the network permeability is shown in Figure 11, where the ratio k_c/k_6 is plotted as a function of C. Here is the network permeability $C = 6$ for k_C, and is the network permeability for values of between 4 and 6 obtained through the removal of chambers and/or channels, starting from the $C = 6$ network. From Eq. 16 it follows that the permeability is proportional to and inversely proportional to $q_T/\Delta p_T$ the network volume, that is

$$\frac{k_C}{k_6} = \frac{(q_T/\Delta p_T)_C}{(q_T/\Delta p_T)_6}\frac{\delta_6}{\delta_C} = \frac{(q_T/\Delta p_T)_C}{(q_T/\Delta p_T)_6}\frac{V_6}{V_C}. \tag{19}$$

To obtain a spatially uniform distribution of coordination numbers, elements are removed randomly with the same probability of removal. Three different cases were studied: removal of chambers and associated channels; removal of oblique and normal channels; and removal of normal channels only.

In the first two cases the permeability decreases with C, due to the decrease in flow paths and subsequent increase in flow resistance, corresponding to lower-values $q_T/\Delta p_T$. Removal of chambers implies that all channels—two oblique and one normal—connected to it are also removed. In the case where channels are removed, either oblique or normal channels are randomly removed with the restriction that each chamber has at least one inlet and one outlet channel. The total number of channels removed to obtain a given value of C is similar in both cases, but removal of chambers implies a lower-value of V_C, a higher value of V_6/V_C, and, thus, higher values of k_C/k_6 than the case of removal of channels only.

In the case of removal of normal channels only, the permeability increases with C, due to the change in network

volume, since the normal channels contribute negligibly to the flow. For a uniform network and assuming that the flow through the normal channels is negligible, it can be shown that the change in permeability is dependent on the network void volume only

$$\frac{k_C}{k_6}=\frac{V_6}{V_C}\approx\frac{2D^3+6d^2l+3d^2l_n}{2D^3+6d^2l+3d^2l_n\alpha}\quad \alpha=\frac{C}{2}-2 \tag{20}$$

This curve is plotted as a solid line in Figure 11 with very good agreement with the simulated values.

Influence of the elements geometry parameters

Factors related to the elements geometric characteristics that may influence the behavior of the network are the average channel and chamber diameters, the average length of the channels and their respective size distributions, measured in terms of the standard deviation. The channels average length l, has only a small effect on the hydrodynamic behavior. Since it only appears on the term R_j^F, it has an impact only for linear flow, when the frictional resistance on the channels is the dominant. This resistance increases proportionally to l, but the void volume also increases, reducing δ, resulting in a small effect of l on the permeability.

The influence of the channels and chambers diameters on the permeability is illustrated in Figure 12 for two sets of values of σ_D and σ_d. The solid lines correspond to a uniform network for which case it can be shown that

$$k=\frac{3\pi\varepsilon}{16\mu}\frac{d^4}{(\pi l+4d)}\frac{(1+D)^2\cos^2\theta}{2D^3+6d^2l+3d^2l_n}. \tag{21}$$

A good agreement is obtained between these curves and the case with narrow diameter distributions, that is for σ_D and $\sigma_d=0.5$. For wider distributions σ_D and $\sigma_d=0.40$, the values of k increasingly deviate from the uniform network lines as d increases. This behavior is due to the restrictions imposed between the values of d and D at the local level, since when the values of d and D are close, it is easier to occur the case $d<D$. In this case, the distribution of the channel diameters shifts toward smaller values, resulting in lower values of k, as observed for values of d/D close to one.

Figure 12a plots k vs. d/D for constant values of either D or d. In the first case d, constant, the permeability steadily increases with d/D as expected; the deviations of the simulated from the uniform network values, for high d/D is again due to small variations in d leading to larger variations in d/D. In the case with d constant, k reaches an asymptotic value for high values of d/D, which is expected since the largest resistance to the flow is associated to the channels. Also, compared to the curve for D constant, the deviations are smaller because they result only of changes in the void volume of the network. For lower values of d/D, the permeability decreases because higher-values of D imply higher-void volumes, and, consequently, higher values of the network thickness δ. In both cases the permeability for higher values of d/D is lower than the uniform network permeability, since the number of channels with diameter smaller than d increases due to the restrictions imposed between the values of d and D at the local level. For large values of σ_D and/or σ_d, the value of

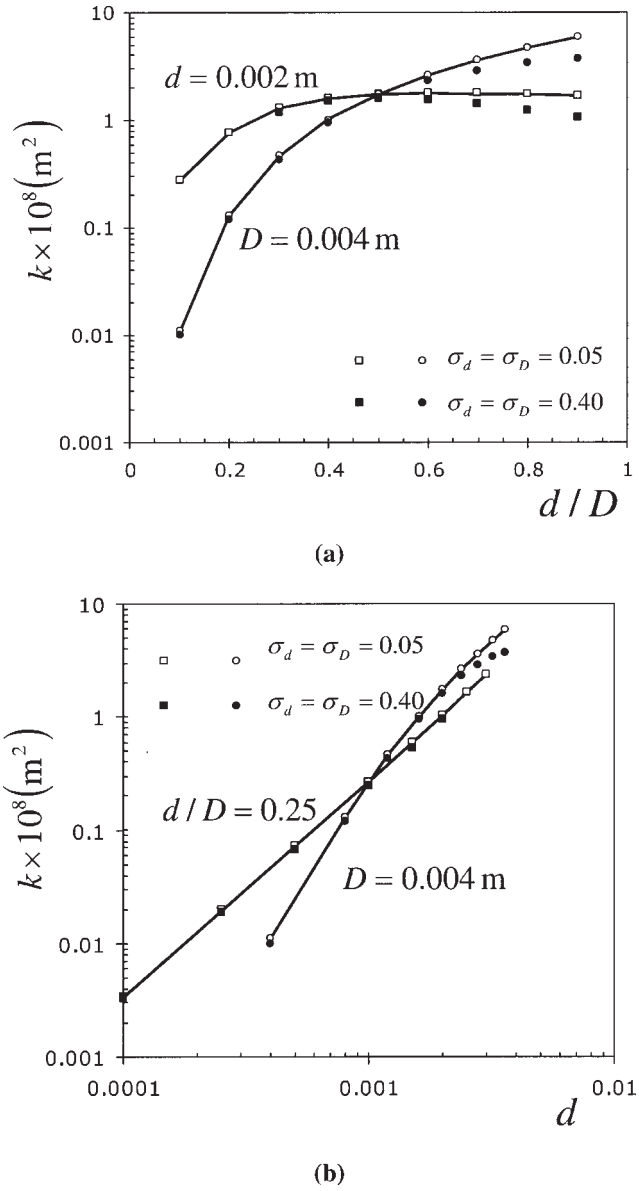

Figure 12. (a) Network permeability *k*, as a function of *d/D*, keeping *d* or *D* constant, and (b) network permeability *k*, as a function of *d*, keeping *d/D* or *D* constant.

k decreases for values of d/D close to one as a result of the application of the restrictions between the values of d and D at the local level.

Figure 12b plots k vs. d for constant values of either D or d/D. The predicted curves are quite different. For constant d/D the permeability increases with d, and it scales with d^2 throughout the entire range of values. However, for constant D it is possible to observe two different zones. For high values of d, the restrictions between the values of d and D at the local level lead to a lower increase in k. As observed in Figure 12a, the deviation between the uniform network and simulated values is larger for $\sigma_d=\sigma_D=0.40$. For low values of the permeability scales with d^3, showing that in the proposed network model the dependence of k on d is a

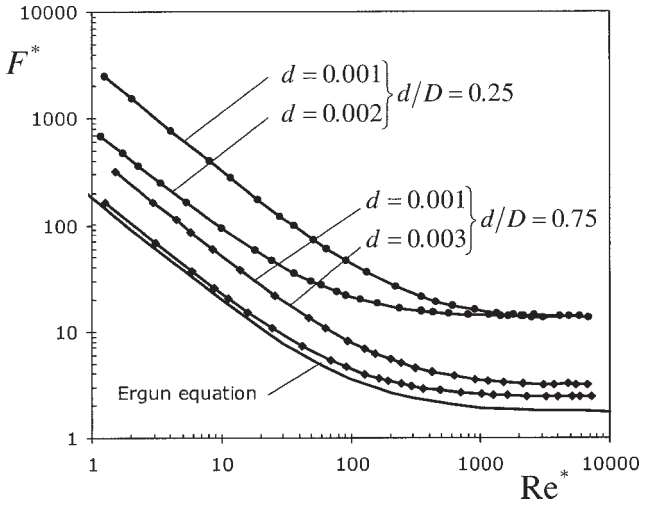

Figure 13. Plot of the modified friction factor *F vs. the modified Reynolds number, for two values.**

function of the characteristic dimensions of the network elements.

Figure 13 shows the plot of F^* vs. Re^* for two values of d/D obtained with different pairs of d and D. For linear flow, the expected behavior is observed: for each pair d/D, and a given Re^*, F^* scales with d^{-4}; the differences between the two sets of curves can be explained as before. For nonlinear flow, the curves for each value of d/D start to approach each other, beginning at the transition zone, and reaching similar asymptotic value of F^* for high Re^*. This result is unexpected, because the resistance of the network branches in all flow regimes has the same functional dependence on the channel diameter, proportional to d^{-4}. However, comparing the expressions for the three resistance terms, some differences do exist. For a uniform network, it is possible to obtain an analytical expression for the ratio between the predicted values of F^* for fixed q_T and d/D, but different pairs of values of d and D. Assuming $C = 6$, and considering only the dominant resistance terms for linear and nonlinear flow, the following expressions are obtained

$$\frac{F_1^*}{F_2^*} = \left(\frac{d_2}{d_1}\right)^4 \left(\frac{\pi l + 4d_1}{\pi l + 4d_2}\right) \left(\frac{l + D_2}{l + D_1}\right) \left(\frac{4D_1^3 + 6d_1 l + 3d_1 l_n}{4D_2^3 + 6d_2 l + 3d_2 l_n}\right)^2 \quad \text{for linear flow} \quad (22)$$

$$\frac{F_1^*}{F_2^*} = \left(\frac{d_2}{d_1}\right)^4 \left(\frac{l + D_2}{l + D_1}\right) \left(\frac{4D_1^3 + 6d_1 l + 3d_1 l_n}{4D_2{}^3 + 6d_2 l + 3d_2 l_n}\right)^2 \quad \text{for non-linear flow} \quad (23)$$

where the indexes 1 and 2 correspond to two distinct pairs of values of d and D. Both expressions are similar and function of the average values for the sizes of the network elements. Although in Figure 13 the results are presented using as F^*; a function of Re^*, it can be shown that the same qualitative behavior is observed when the results are presented using F^* as a function of q_T. Similar expressions can be obtained for the ratio between values of F^* keeping constant, but these turn out to be functions of q_T, and do not allow a direct comparison of the results.

These expressions predict quite accurately the ratio F_1^*/F_2^* observed in Figure 13, showing that the differences in the observed behavior are the result of changes on the dominant terms of the flow resistance of the network branches due to a transition in the flow regimen.

Other effects may be relevant to the change of behavior between linear and nonlinear flow. Figure 14 shows the distributions of v_j in the oblique channels for linear and nonlinear flow, where, in order to directly compare both distributions, the velocity values have been normalized by the highest velocity value observed in each case v_{max}. Results show that the velocity distribution is narrower for nonlinear-flow conditions, revealing that the changes on the main resistance terms also have an effect on the characteristics of the flow at the local level. This type of behavior has been predicted[66] for flow through a porous medium formed by rough fractures in the transition between linear and nonlinear flow, and the results obtained for the velocity distributions agree qualitatively with the experimental results of Sederman et al.[67] These authors determined experimentally the velocity distributions in packed beds made from glass spheres of about 5 mm in diameter using magnetic resonance imaging (MRI), and have shown the existence of a tail with negative (direction of flow opposite to the main direction of the flow) values for the velocity, as it is also predicted by the network model.

Comparison with published data

The validation of the network model with experimental data requires that both the hydrodynamic and the geometrical models be used simultaneously. According to the limitations of the geometrical model, only data obtained in packed beds formed by spheres with a narrow distribution of diameters can be considered. Since in most cases the reported data does not include information on the pore-size distributions, the following analysis was done using uniform networks. The geometric model assumes only two values of the coordination number, $C = 4$ and 6. Although, in real-porous media

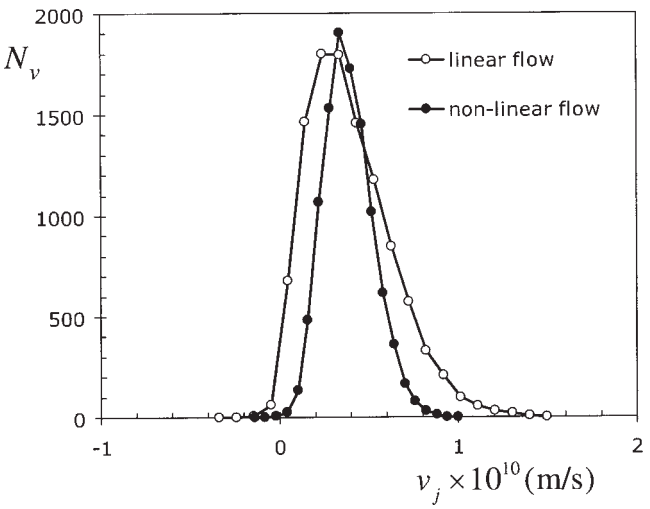

Figure 14. Distributions of the normalized channels-fluid velocity v_j/v_{max}, for linear and nonlinear flow.

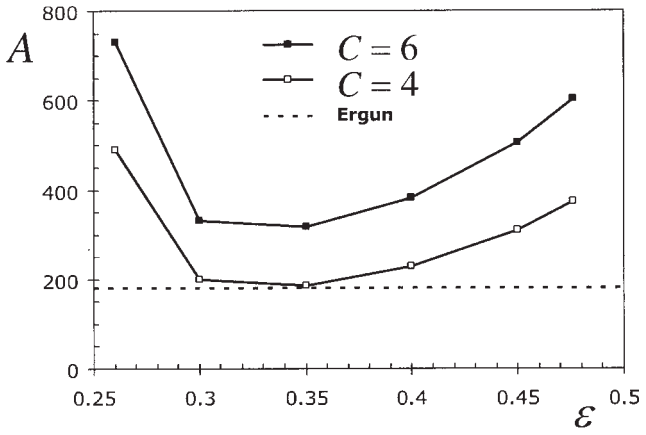

(a)

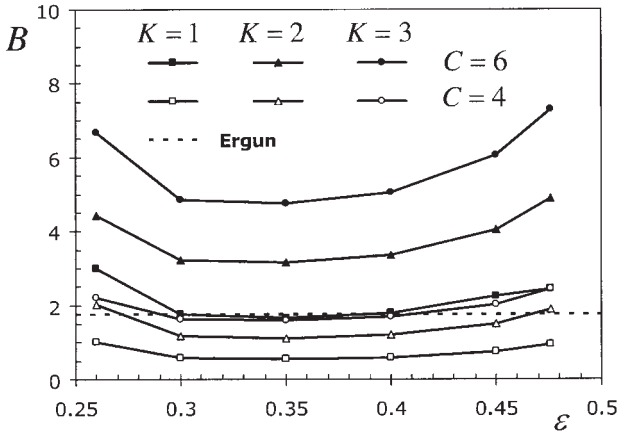

(b)

Figure 15. Ergun equation constants *A* and *B*, vs. the porosity ε for different values of *C* and *K*.

a distribution of values of C is likely, the previous restriction of narrow distribution of diameters implies low-spatial variations in the value of C.[55]

Given the data for a particular packed bed, namely the porosity and the particle diameter, and assuming a value for C, it is possible to predict the values of the permeability and the constant. To obtain the value of a value of must also be given.

Figure 15 plots the Ergun-equation constants, A and B, as functions of the porosity ε, compared with the corresponding values obtained by Ergun. The parameter represents the influence of the viscous forces on the flow through a packed bed, and it is expected to decrease slightly as ε increases.[4] Figure 15a shows that A decreases sharply in the range $0.25 \leq \varepsilon < 0.3$, takes a nearly constant value for $0.3 \leq \varepsilon \leq 0.4$, and it increases slightly for $\varepsilon > 0.4$. For $C = 0.4$, and in the intermediate range of porosities the simulated values are close to the published value of $A = 180$.[4] Similar behavior is observed for B (Figure 15b), but now with a large spread of the values K depending on and a larger dependence on the value of $A = C$. Similarly to the results obtained for A, the best agreement with the value of suggested by MacDonald and coworkers[4] is observed for $C \approx 4$, and values of K around 4. Thus, the results show that the values of should be higher than 1.5, confirming the above predictions.

The PTT1 and PTT2[18] datasets and six other sets of data from Kim,[58] referred as KIM1, KIM2, KIM3, KIM4, KIM5 and KIM6, were used to compare experimental data with results predicted by the network model. In the datasets KIM1, KIM2 and KIM3 particles with a single size were used, while in datasets KIM4, KIM5 and KIM6 mixtures of uniform particle sizes were considered. The geometrical model relationships were used to obtain the network elements average sizes using the reported experimental values and as shown in Table 2. Table 3 compares the reported experimental data, k_{exp}, with the corresponding simulated values for $C = 4$ and $C = 6$, $k_{C=4}$ and $k_{C=6}$.

Results show that for the PTT1 and PTT2 datasets $k_{exp} > k_{C=4}$, while for all 6 KIM datasets $k_{exp} \approx k_{C=4}$. Assuming that k is a function of C only, and that only normal channels are removed to change C, Eq. 20 may be used to obtain the values of C, so that $k_{exp} = k_C$, which are also shown in Table 3. For the PTT datasets, $C = 3$ or lower, but for the other 6 datasets $C \approx 4$, which is the value generally assumed to be found in packed beds. For example, Sederman and coworkers,[47] based on the characterization of the local structure in a packed bed, made from uniform sized-glass spheres with a diameter of 5 mm, found C that has distribution of values with an average value between 4 and 5. Other experimental results using different techniques, such as image analysis,[68] characterization of the local structure of simulated-packed beds,[69] and MRI,[47,67,70] all agree that the average coordination number of packed beds made from uniform-size particles is between 4 and 5.

Table 3. Experimental and Calculated Data for Permeability *k*, Ergun Constants *A* and *B*, and the *K* Coefficients

	Experimental Data			Calculated Data								
				$k_C \times 10^9$ (m^2)			*A*		*B*		*K*	
Set	$k_{exp} \times 10^9$ (m^2)	*A*	*B*	$C = 4$	$C = 6$	C ($k_C = k_{exp}$)	$C = 4$	$C = 6$	$C = 4$	$C = 6$	$C = 4$	$C = 6$
PPT1	0.233	–	–	0.173	0.103	2.29	–	–	–	–	–	–
PPT2	0.628	–	–	0.527	0.325	3.00	–	–	–	–	–	–
KIM1	2.53	184.2	1.93	2.55	1.50	4.04	190.6	322.9	0.832	3.39	3.48	1.21
KIM2	5.67	177.8	1.90	5.58	3.30	3.92	192.4	325.8	0.835	2.39	3.42	1.19
KIM3	9.88	174.0	1.81	9.87	5.83	3.99	191.8	324.8	0.834	2.39	3.26	1.13
KIM4	7.06	180.6	1.92	7.25	4.28	4.13	186.2	315.4	0.828	2.38	3.48	1.21
KIM5	5.27	183.5	1.94	5.51	3.52	4.24	184.6	312.9	0.827	2.37	3.52	1.22
KIM6	3.71	179.5	1.88	3.82	2.26	4.14	184.0	311.7	0.827	2.37	3.41	1.19

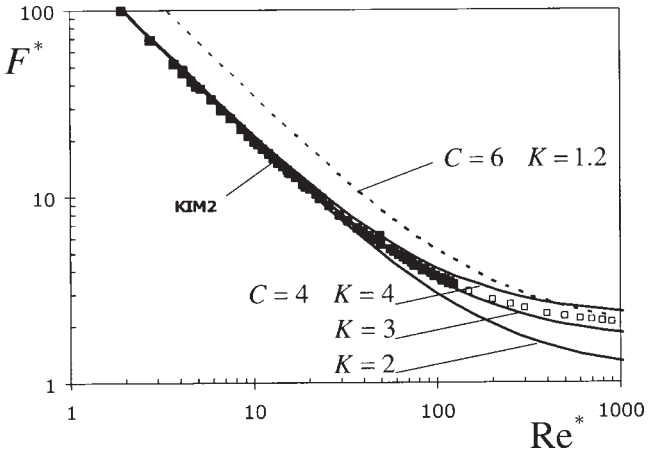

Figure 16. Comparison between experimental data from Kim[65] and simulated values for suitably chosen values of *C* and *K*.

The datasets from Kim[58] also include experimental data for nonlaminar flow. Therefore, it is possible to make a direct comparison between the values predicted by the network model, and the experimental values of the constants A and B. In Table 3 A_{exp} and B_{exp} are presented and compared to the corresponding calculated A_c, for $C = 4$ and $C = 6$, assuming $K = 1.5$. As expected, the values of show the same qualitative behavior observed when comparing the predicted and experimental values of permeability.

For B, the experimental values also fall between the values predicted for $C = 4$ and $C = 6$. However, for $C = 4$, the agreement with the experimental data is not as good as the agreement observed for the values of A. Also, for $C = 6$ the values of B are much larger than the experimental values. So, based on these results it can be concluded that assuming a value of $K = 1.5$ is not representative of the flow conditions inside these packed beds.

Using the 6 KIM datasets, the values of K that verify B_{exp}, were determined and are shown in Table 3, where a strong influence of C can be observed. The results for predict $C = 6$ values of C lower than 1.5, in agreement with correlations available in the literature for simple contractions and expansions.[62] On the other hand, the calculations for both k and A strongly suggest a value of $C = 4$, and the existence of more than one inlet and outlet associated with most chambers of the network, and the mixing between the streams in the chambers should result in values of K larger than 1.5.

The Kim[58] datasets also show the full curves of the pressure drop vs. the volumetric flow rate. Figure 16 shows the experimental data points (dark symbols) for the KIM2 dataset, together with simulated curves for suitably chosen values of C and K. The dataset was extended to higher values of Re^* (open symbols) using the reported values of A and B, to ease the comparison between experimental and predicted values. For $C = 6$ and $K = 1.2$, the match between the experimental points and the simulated (dashed) is good for high-Reynolds numbers, but it is very poor for laminar regime. For $C = 4$ the match for low Re^* is good for any of the values of $K = 2$, 3 and 4. For high-values of Re^*, a good match is obtained for $K \approx 3$, in agreement with the value of $K = 3.48$ obtained from the experimental value of B (see Table 3). Also, it is $K \approx 3$ for that the best concordance between experimental and predicted results is observed for all flow regimens, in particular in the transition zone.

Conclusions

A 2-D network model consisting of two types of interconnected elements for the description of transport phenomena in packed beds has been developed. A geometrical model that relates real packing data, such as the porosity and average-particle diameter, with the network elements-size distributions has been described. Good comparison between predicted and experimental values of the characteristics dimensions of the network elements is verified for packed beds consisting of particles with narrow-size distributions.

Using this network model, a flow simulator based on an electric analogue has been implemented, which is capable of describing single-phase flow in all regimes, from laminar to turbulent. The flow model takes into account not only friction effects within the channels but also inertial effects due to the interconnections between the different types of elements. The inclusion of these terms is essential for the model to be able to describe linear and nonlinear flows, as well the transition zone.

The model and simulator were used to characterize the influence of the network characteristics on the flow field. Results showed that the main factor controlling the flow at the local level are the characteristic dimensions of the channels, in particular the diameter, and the spatial regularity of the network. It was found that the spatial distribution of the oblique channels is the main factor influencing the flow field, and that, in the estimation of the parameters that describe the flow at the macroscopic level (for example, the permeability), the variations of the void volume of the network must be accounted for.

Simulated and calculated data were successfully compared with experimental data available in the literature. The influence of the mean coordination number on the permeability, and on the value of K was studied. Results show that the best agreement with the experimental data are obtained when $C = 4$ and $K > 1.5$.

Acknowledgments

Financial support for this work was in part provided by national research grants 3/3.1/GEG/2564/95 and FCT/POCTI/EQU/34151/99 for which the authors are thankful. A.A. Martins and P.E. Laranjeira acknowledge their Ph.D. scholarships by FCT, PRAXIS XXI/BD/2631/93 and PRAXIS XXI/BD/21490/99, respectively.

Literature Cited

1. Dullien FAL. *Porous Media. Fluid Transport and Pore Structure*. 2nd ed: Academic Press; 1992.
2. Sahimi M. *Flow and Transport in Porous Media and Fractured Rock. From Classical Methods to Modern Approaches*. Weinham: VCH; 1995.
3. Ergun S, Fluid flow through packed columns. *Chem Eng Progress*. 1995;48:89–94.
4. Macdonald IF, El-Sayed MS, Mow K, Dullien FAL. Flow through porous media. The Ergun equation revisited. *Ind Eng Chem Fund*. 1979;18:199–208.

5. Comiti J, Renaud M. A new model for determining mean structure parameters of fixed beds from pressure drop measurements: application to beds packed with parallelepipedal particles. *Chem Eng Sci*. 1989;44:1539–1549.
6. Panigrahi MR, Murty JS. A generalized spherical multi-particle model for particulate systems: fixed and fluidized Beds. *Chem Eng Sci*. 1991;46:1863–1868.
7. Liu S, Afacan A, Masliyah J. Steady incompressible laminar flow in porous media. *Chem Eng Sci*. 1994;49:3565–3586.
8. Puncochar M, Drahos J, Limits of applicability of capillary model for pressure drop correlation. *Chem Eng Sci*. 2000;55:3951–3954.
9. Adler PM. *Porous Media. Geometry and Transport*. Boston: Butterworth-Heinemann; 1992.
10. Happel J. Viscous flow in multiparticle systems: slow motion of fluids relative to beds of spherical particles. *AIChE J*. 1958;4:197–201.
11. Sangani AS, Acrivos A. Slow flow past periodic arrays of cylinders with application to heat transfer. *Int J Multiphase Flow*. 1982;8:193–206.
12. Zick AA, Homsy GM. Stokes flow through periodic arrays of spheres. *J Fluid Mech*. 1982;115:13–25.
13. Quintard M, Whitaker S. Transport in ordered and disordered porous media: volume-averaged equations: closure problems and comparison with experiment. *Chem Eng Sci*. 1993;48:2537–2564.
14. Dwyer HA, DeBus K, Shahcheraghi N. The use of oversets meshes in particle and porous media: three-dimensional flows. *Int J Numerical Methods Fluids*. 1999;31:399–406.
15. Liang Z, Ioannidis MA, Chatzis I. Permeability and electrical conductivity of porous media from 3D stochastic replicas of the microstructure. *Chem Eng Sci*. 2000;55:5247–5262.
16. Berkowitz B, Ewing RP. Percolation theory and network modelling. Applications in soil physics. *Surveys Geophysics*. 1998;19:23–72.
17. Dullien FAL. Single phase flow through porous media and pore structure. *Chem Eng J*. 1975;10:1–34.
18. Payatakes AC, Tien C, Turien RM. A new model for granular porous media. *AIChE J*. 1973;19:58–76.
19. Blick EF. Capillary-orifice model for high-speed flow through porous media. *Ind Eng Chem Proc Dev*. 1966;5:90–94.
20. Neira MA, Payatakes AC. Collocation solution of creeping newtonian flow through periodically constricted tubes with piecewise continous wall profile. *AIChE J*. 1978;24:43–54.
21. Venkatesan M, Rajagoplan R. A hyperboloidal constricted tube model of porous media. *AIChE J*. 1980;26:694–698.
22. Pendse H, Chiang H, Tien C. Analysis of transport processes with granular media using the constricted tube model. *Chem Eng Sci*. 1983;38:1137–1150.
23. Lahbabi A, Chang H. Flow in periodically constricted tubes: transition to inertial and nonsteady flows. *Chem Eng Sci*. 1986;41:2487–2505.
24. Hemmat M, Borhan A. Creeping Flow trough sinusoidally constricted capillaries. *Physics of Fluids*. 1995;7:2111–2221.
25. Thompson KE, Fogler HS. Modelling flow in disordered packed beds from pore-scale fluid mechanics. *AIChE J*. 1997;43:1377–1389.
26. Thauvin F, Mohanty KK. Network modelling of non-Darcy flow through porous media. *Transport in Porous Media*. 1998;31:19–37.
27. Wang X, Thauvin F, Mohanty KK. Non-Darcy flow through anisotropic porous media. *Chem Eng Sci*. 1999;54:1859–1869.
28. Koplik J. Creeping flow in two-dimensional networks. *J Fluid Mech*. 1982;119:219–247.
29. Ioannidis MA, Chatzis I. Network modelling of pore Structure and transport properties of porous media. *Chem Eng Sci*. 1993;48:951–972.
30. Fatt M. The network model of porous media. I – Capillary pressure characteristics. *Petroleum Transactions*. 1956;207:142–164.
31. Dias MM, Payatakes AC. Network models for two-phase flow in porous Media. Part 1: immiscible displacement of non-wetting fluids. *J Fluid Mech*. 1986;164:305–336.
32. Dias MM, Payatakes AC. Network models for two-phase flow in porous Media. Part 2. Motion of Oil Ganglia. *J Fluid Mech*. 1986;164:337–358.
33. Chu CF, Ng KM. Flow in packed beds with a small tube to particle diameter ratio. *AIChE J*. 1989;35:148–158.
34. Constantinides GN, Payatakes AC. A three dimensional network model for consolidated porous media: basic studies. *Chem Eng Comm*. 1989;81:55–81.
35. Constantinides GN, Payatakes AC. Network simulation of steady-state two-phase flow in consolidated porous media. *AIChE J*. 1996;42:369–382.
36. Androutsopoulos GP, Mann R. Evaluation of mercury porosimeter experiments using a network pore structure model. *Chem Eng Sci*. 1979;34:1203–1212.
37. Mata VG, Lopes JCB, Dias MM. Porous media characterization using mercury porosimetry simulation. 1: Description of the simulator and its sensitivity to model parameters. *Ind & Eng Chem Res*. 2001;40:3511–3522.
38. Mata VG, Lopes JCB, Dias MM. Porous media characterization using mercury porosimetry simulation. 2. An iterative method for the determination of the real pore size distribution and the mean coordination number. *Ind & Eng Chem Res*. 2001;40:4386–4843.
39. Koplik J, Lasseter TJ. One and two phase flow in network models of porous media. *Chem Eng Comm*. 1984;26:285–295.
40. Melli TR, Scriven LE. Theory of two phase cocurrent downflow in networks of passages. *Ind & Eng Chem Res*. 1991;30:951–969.
41. Chan SK, Ng KM. Geometrical characteristics of a computer-generated three-dimensional packed column of equal and unequal sized spheres – with special reference to wall effects. *Chem Eng Comm*. 1986;48:215–236.
42. Spedding M, Spencer K. Simulation of packing density and liquid flow in fixed beds. *Comp Chem Eng*. 1995;19:43–73.
43. Bryant S, Blunt M. Prediction of relative permeability in simple porous media. *Physical Reviews A*. 1992;46:2004–2011.
44. Bryant SL, King PR, Mellor DW. Network model evaluation of permeability and spatial correlation in a real random sphere packing. *Transport in Porous Media*. 1993;11:53–70.
45. Nolan GT, Kavanagh PE. The size distribution of interstices in random packings of spheres. *Powder Technol*. 1994;78:231–238.
46. Gallegos DP, Smith DM. A NMR technique for the analysis of pore structure: determination of continous pore size distributions. *J Colloid Interf Sci*. 1988;122:143–153.
47. Sederman AJ, Johns ML, Bramley AS, Alexander P, Gladden LF. Magnetic resonance imaging of liquid flow and pore structure within packed beds. *Chem Eng Sci*. 1997;52:2239–2250.
48. Manz B, Gladden LF, Warren PB. Flow and dispersion in porous Media: lattice-boltzmann and NMR studies. *AIChE J*. 1999;45:1845–1854.
49. Stephenson JL, Stewart WE. Optical measurements of porosity and fluid motion in packed beds. *Chem Eng Sci*. 1986;41:2161–2170.
50. Bey O, Eigenberger G. Fluid flow through catalyst filled tubes. *Chem Eng Sci*. 1997;52:1365–1376.
51. Giese M, Rottschäfer K, Vortmeyer D. Measured and modelled superficial flow profiles in packed beds with liquid flow. *AIChE J*. 1998;44:484–490.
52. Pietsch W. Successfully use agglomeration for size Enlargement. *Chem EngProgress*. 1996;92:29–45.
53. Comiti J, Renaud M. A new model for determining mean structure parameters of fixed beds from pressure drop measurements: application to beds packed with parallelepipedal particles. *Chem Eng Sci*. 1989;44:1539–1549.
54. Liu S, Masliyah JH. Single phase fluid flow in porous media. *Chem Eng Comm*. 1996;148–150:653–732.
55. Chan SK, Ng KM. Geometrical characteristics of the pore space in a random packing of spheres. *Powder Technol*. 1988;54:147–155.
56. Mayer RP, Stowe RA. Mercury porosimetry: breakthrough pressure for penetration between packed spheres. *J of Colloid Sci*. 1965;20:893–911.
57. Mayer RP, Stowe RA. Mercury porosimetry: filling of toroidal void volume following between packed spheres. *J Phys Chem*. 1966;70:3867–3873.
58. Kim BYK. *The resistance to flow in simple and complex porous media whose matrices are composed of spheres*. University of Hawai at Manoa; 1985. M.Sc. Thesis.
59. Desoer CA, Kuh ES. *Basic Circuit Theory*, New York: McGraw-Hill; 1969.
60. Shah CB, Yortsos YC. Aspects of flow of power-law fluids in porous media. *AIChE J*. 1995;41:1099–1112.
61. Lim CS, Ti HC. Mixed specification problems in large-scale pipeline networks. *Chem Eng J*. 1998;71:23–35.
62. White FM. *Fluid Mechanics*, 3rd Ed. Mac-Graw Hill; 1994.

63. Niven AA. Physical insight into the Ergun and Wen & Yu equations for fluid flow in packed and fluidized beds. *Chem Eng Sci*. 2002;57:527–534.
64. Fand RM, Kim BYK, Lam ACC, Phan RT. Resistance to the flow of fluids through simple and complex porous media whose matrices are composed of randomly packed spheres. *J Fluids Eng. — Trans. ASME*. 1987:109;268–274.
65. Kececioglu I, Jiang Y. Flow through porous media of packed beds saturated with water. *J Fluids Eng. — Trans. ASME*. 1994;116:164–170.
66. Skjetne E, Hansen A, Gudmundsson JS. High velocity in a rough fracture. *J Fluid Mechanics* 1999;383:1–28.
67. Sederman AJ, Johns ML, Alexander P, Gladden LF. Structure-flow correlations in packed beds. *Chem Eng Sci*. 1998;53:2117–2128.
68. Yanuka M, Dullien FAL, Elrick DE. Percolation processes and porous media. I— Geometrical and topological model of porous media using a three-dimensional joint pore size distribution. *J Colloid Interf Sci*. 1986;112:24–41.
69. Al-Raoush R, Thompson K, Willson CS. Comparison of network generation techniques for unconsolidated porous media. *Soil Sci Soc Am J*. 2003;67:1687–1700.
70. Baldwin CA, Sederman AJ, Mantle MD, Alexander P, Gladden LF. Determination and characterization of a pore space from 3D volume images. *J Colloid Interf Sci*. 1996;181:79–92.

Appendix

The upper limit log normal (ULLN) distribution function results from a transformation of the Gaussian or normal distribution function

$$f(\xi) = \frac{1}{\sigma\sqrt{2\pi}} \exp\left[-\frac{1}{2}\left(\frac{\xi-\mu}{\sigma}\right)^2\right] \qquad -\infty < \xi < +\infty \quad \text{(A1)}$$

where μ is the distribution mean value and is the standard deviation, resulting in

$$f(\eta) = \frac{\delta}{\sqrt{\pi}} \exp[-\delta^2\eta^2] \qquad -\infty < \eta < \infty \quad \text{(A2)}$$

where δ is parameter, η and ξ are related by

$$\eta = \ln\left(\frac{a\xi}{\xi_{\max}-\xi}\right) \qquad -\infty < \eta < \infty \quad \text{(A3)}$$

and a and $\xi_{\max}$ are two additional parameters. The ULLN distribution function, expressed in terms of ξ, can be obtained by means of a statistics theorem for a function of random variables that relates the one-to-one correspondence between ξ and η, in the form $f(\eta) = f(\xi)|d\xi/d\eta|$, resulting in

$$f(\xi) = \frac{\delta\xi_{\max}}{\sqrt{\pi}\xi(\xi_{\max}-\xi)} \exp\left[-\delta^2 \ln^2\left(\frac{a\xi}{\xi_{\max}-\xi}\right)\right] \qquad -0 < \xi < \xi_{\max} \quad \text{(A4)}$$

Imposing that average value of the ULLN distribution is equal to μ, it can be shown that when $a \approx \xi_{\max} - 1$, its shape is approximately Gaussian, but limited to the range $-0 < \xi < \xi_{\max}$.

Manuscript received Feb. 10, 2006, and revision received Aug. 4, 2006, and final revision received Oct. 15, 2006.